

Cost-Effective XL-MIMO Communication with Cylinder Directly-Connected Antenna Array

Xuancheng Zhu, *Student Member, IEEE*, Zhiwen Zhou, Zhenjun Dong, *Student Member, IEEE*, and Yong Zeng, *Fellow, IEEE*

Abstract—Extremely large-scale multi-input multi-output (XL-MIMO) is a promising technology for the sixth generation (6G) wireless networks, thanks to its superior spatial resolution and beamforming gains. In order to realize XL-MIMO cost-effectively, an innovative *ray antenna array* (RAA) architecture with directly-connected *uniform linear array* (ULA) was recently proposed, which achieves flexible beamforming without relying on traditional analog phase shifters or digital beamforming. However, RAA suffers from the signal blockage issue since its ray-configured ULAs are placed in the same plane. To address this issue, this paper proposes a novel antenna array architecture termed *cylinder directly-connected antenna array* (DCAA), which is achieved via multiple *simple uniform circular array* (sUCA) with carefully designed orientations in a layered three-dimensional structure. The so-called sUCA partitions the *uniform circular array* (UCA) into two sub-arrays where each sub-array has all antenna elements directly connected to achieve a desired beam direction corresponding to the sub-array's physical orientation, thus achieving full spatial coverage. Compared with the conventional ULA architecture with hybrid analog/digital beamforming (HBF), the proposed cylinder DCAA can achieve uniform spatial resolution, enhanced communication rate and lower hardware costs. Simulation results are provided to validate the promised gains of cylinder DCAA, demonstrating its great potential for high-frequency systems such as millimeter wave (mmWave) and Terahertz (THz) systems.

Index Terms—XL-MIMO, DCAA, flexible beamforming, mmWave communication, THz communication.

I. INTRODUCTION

OVER the past few decades, multi-input multi-output (MIMO) technology has served as a cornerstone in the evolution of wireless communications [2]. From the fourth-generation (4G) to the fifth-generation (5G) mobile communication networks, multi-antenna technology has evolved from MIMO (typically with 8 antenna elements) to massive MIMO (typically with 64 antenna elements), to substantially enhance spectral efficiency, reliability and connection density. For the sixth-generation (6G) mobile communication networks, more ambitious goals have been envisioned, such as centimeter-level positioning accuracy, ultra-high connection density, and ultra-low latency on the order of 0.1–1 ms [3], [4]. To meet these goals, various new MIMO technologies, such as extremely-large scale MIMO (XL-MIMO) [5], sparse MIMO [6] and

cell-free MIMO [7] are being actively explored. In particular, attributing to the extremely large number of antenna elements, XL-MIMO achieves higher beamforming gain, better spectral efficiency and more precise sensing and localization ability. With the growing trend of utilizing higher frequency bands for 6G networks, such as millimeter wave (mmWave) and Terahertz (THz), the practical implementation of XL-MIMO faces significant challenges, including the high hardware costs associated with pricey front-end radio frequency (RF) components, increased signal processing complexity and the difficulty of designing and fabricating advanced components, such as high-precision phase shifters. These factors collectively hinder the practical implementation of XL-MIMO. Therefore, it is necessary to develop innovative and cost-effective antenna array structures.

Since RF chains and front-end components account for a substantial portion of hardware costs [8], [9] and power consumption, an effective strategy to realize XL-MIMO is to reduce the number of RF chains or adopt more efficient front-end components [10]. For instance, hybrid analog/digital beamforming (HBF) [11], lens antenna array [12], movable antenna array [13] or fluid antenna systems [14] and reconfigurable tri-hybrid MIMO antenna array [15] have been investigated. However, for HBF and reconfigurable tri-hybrid MIMO, the required number of phase shifters increases with the number of antennas, which is huge for XL-MIMO systems. Besides, HBF requires complicated control systems for accurate and dynamic phase control, thus increasing hardware complexity and power consumption. For lens antenna, dielectric lenses are difficult to integrate with multiple antenna techniques due to their bulky size and high insertion loss [16]. For XL-MIMO based on movable antenna or fluid antenna array, accurate channel state information (CSI) is challenging to be estimated [17]. Besides, extra bulky mechanical controls need to be introduced, which compromises the cost-efficiency, power consumption and response time.

To address the above issues, an innovative multi-antenna architecture termed *ray antenna array* (RAA) was recently proposed, which offers a promising solution to simultaneously reduce hardware cost and enhance system performance [18], [19]. As illustrated in Fig. 1(a), the RAA architecture consists of a large number of low-cost antenna elements arranged into a ray-like structure, where each ray corresponds to a *simple uniform linear array* (sULA) with a carefully designed orientation. All antenna elements within each sULA are directly connected, so that each sULA is able to form a beam aligned with its physical orientation. With the assistance of

Part of this work will be presented at 2025 IEEE Globecom, the 6th workshop on emerging topics in 6G communications, 2025. [1]

X. Zhu, Z. Zhou, and Y. Zeng are with the National Mobile Communications Research Laboratory, Southeast University, Nanjing 210096, China. Y. Zeng is also with the Purple Mountain Laboratories, Nanjing 211111, China (e-mail: {213223563, zhiwen_zhou, yong_zeng}@seu.edu.cn). Z. Dong is with the Purple Mountain Laboratories, Nanjing 211111, China (e-mail: dongzhenjun@pmlabs.com.cn). (Corresponding author: Yong Zeng.)

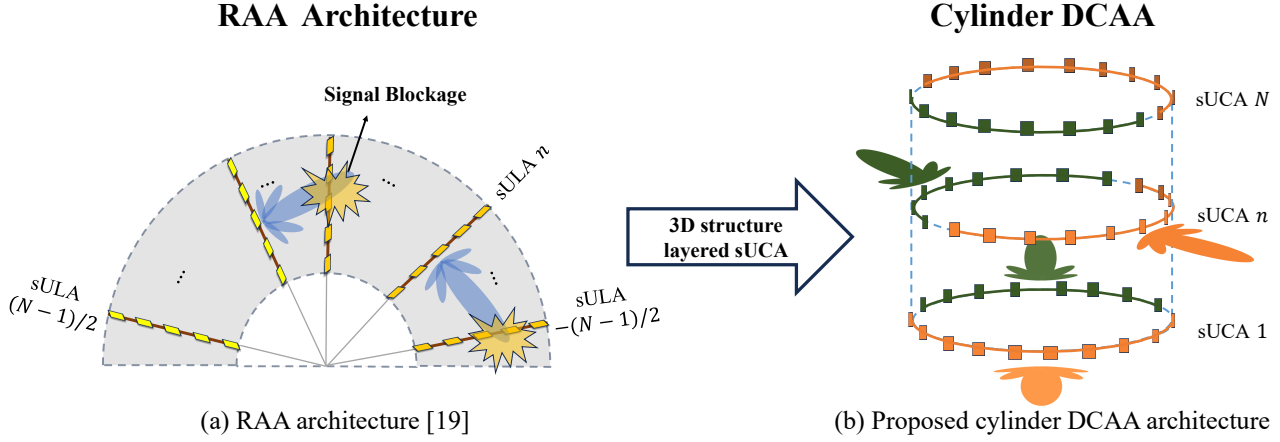


Fig. 1. RAA architecture and the proposed cylinder DCAA architecture, which addresses the signal blockage issue by arranging multiple sUCAs in a layered 3D structure.

a ray selection network (RSN), RAA can achieve uniform spatial resolution, enhanced beamforming gain, high-precision sensing and reduced hardware costs [19], [20], though at the expenditure of more bulky array size. However, when multiple sULAs are deployed on the same two-dimensional (2D) plane with different orientations, the RAA architecture may suffer from signal blockage issue among different sULAs. Specifically, the beam generated by a sULA propagates directly toward its forward direction, where adjacent sULAs are located, thereby physically obstructing the transmitted signals, as illustrated in Fig. 1(a).

To address the aforementioned signal blockage issue in the RAA architecture, this paper proposes a novel antenna array design, referred to as cylinder *directly-connected antenna array* (DCAA). As illustrated in Fig. 1(b), the proposed cylinder DCAA arranges multiple differently orientated *simple uniform circular arrays* (sUCAs) into a three-dimensional (3D) layered structure. The so-called sUCA partitions the antenna elements equally into two complementary semi-circular-configured sub-arrays, and each sub-array has the antenna elements directly connected with the variable length antenna delay line technology. Through the selection matrix, sub-arrays of all sUCAs in the cylinder DCAA are selectively connected with few RF chains for further digital baseband processing. Thanks to the 3D layered structure, the cylinder DCAA can effectively avoid physical blockage among arrays, thereby resolving the signal blockage issue inherent in the RAA architecture. The main contributions of this paper are summarized as follows.

- First, we present the overall system model of cylinder DCAA in Section II and the geometric structure and the array response pattern of sUCA in Section III, which is the basic component of the proposed cylinder DCAA. Composed of two complementary sub-arrays, the sUCA incorporates the direct RF connections utilizing variable length antenna delay lines for the antenna elements within each sub-array to achieve desired beam directions without analog beamforming technology. We provide a comprehensive mathematical analysis of the response pattern of

sUCA's sub-arrays with any given orientation. The study demonstrates that the sUCA's sub-arrays achieve desired spatial resolution and low side-lobe levels, making them suitable for constructing more complex array structures.

- Second, the detailed parameters design of the proposed cylinder DCAA is derived in Section IV-A and IV-B based on the characteristics of sUCA. The cylinder DCAA is constructed by stacking multiple sUCAs vertically into a layer-configured structure, with each sUCA consisting of two complementary sub-arrays with carefully designed orientations to achieve uniform spatial resolution and avoid physical blockage among sub-arrays. Since the antenna elements within each sub-array of sUCAs are directly connected without using any phase shifters, the proposed cylinder DCAA significantly reduces hardware costs and implementation difficulty compared to the classic HBF architectures. The resulting cylinder DCAA provides enhanced beamforming gains, uniform spatial coverage, and improved cost-efficiency, making it a promising solution for flexible beamforming, especially for high frequency systems like mmWave or THz systems in 6G networks.
- Finally, detailed input-output signal models for the proposed cylinder DCAA in both uplink and downlink communication scenarios are derived in Section V. We evaluate the communication performance of the cylinder DCAA in terms of signal-to-interference-plus-noise ratio (SINR) and maximum sum rate, comparing it with a cell sectoring system based on ULA with HBF. Simulation results in Section VI-A and VI-B reveal that the proposed cylinder DCAA achieves superior communication rates, particularly in dense connectivity scenarios, thanks to the uniform spatial resolution. Additionally, a cost analysis in Section VI-C highlights that the cylinder DCAA is more cost-efficient than cell sectoring based on ULA with HBF, making it a practical and scalable solution for future 6G networks.

Notation: Italic, bold-faced lower- and upper-case letters

denote scalars, vectors, and matrices, respectively. The transpose and Hermitian transpose operation are given by $(\cdot)^T$ and $(\cdot)^H$, respectively. $\mathbb{C}^{M \times N}$ and $\mathbb{R}^{M \times N}$ signify the spaces of $M \times N$ complex and real matrices. $\text{diag}(\mathbf{a})$ denotes a diagonal matrix with its diagonal entries composed from the vector \mathbf{a} in sequence. \mathbb{Z} denotes the space of integers. $\mathbf{1}_{M \times N}$ represents an $M \times N$ matrix with all entries equal to 1. $j = \sqrt{-1}$ denotes the imaginary unit of complex numbers. The distribution of a circularly symmetric complex Gaussian (CSCG) random variable with mean 0 and variance σ^2 is denoted by $\mathcal{CN}(0, \sigma^2)$, and $\mathcal{N}(0, \sigma^2)$ denotes the real-valued Gaussian distribution. $\mathcal{U}(a, b)$ denotes the continuous uniform distribution at the interval $[a, b]$. $|\cdot|$ denotes the absolute value of a scalar. $\|\cdot\|$ denotes the l_2 norm of a vector. $\lceil \cdot \rceil$ and $\lfloor \cdot \rfloor$ denote the ceiling and floor operations, respectively. \odot represents the Hadamard product. $\sup\{\cdot\}$ and $\inf\{\cdot\}$ denote the supremum and the infimum of a set, respectively. $\angle(\cdot)$ denotes the main phase of a complex scalar. $\text{Re}(\cdot)$ and $\text{Im}(\cdot)$ denote the real component and the imaginary component of a complex scalar, respectively. $(\cdot)^*$ denotes the conjugate of a complex scalar or vector. $\mathbb{E}[\cdot]$ denotes the mathematical expectation of a random scalar.

II. SYSTEM MODEL

As shown in Fig. 2, we consider a wireless communication system with N_{RF} RF chains supporting K users, where $K \leq N_{\text{RF}}$. HBF is a classic architecture to meet such a requirement by combining low-dimensional baseband digital beamforming with high-dimensional analog beamforming. However, for mmWave or THz XL-MIMO systems for 6G networks, the required large number of high-precision front-end RF components are expensive and hard to fabricate, which inevitably increases hardware costs and therefore hinders the practical implementation of XL-MIMO. To address this problem, a recently proposed RAA structure reduces hardware costs while enhancing wireless performance by achieving uniform spatial resolution and satisfying beamforming gain through the innovative ray-like array structure [19]. However, as illustrated in Fig. 1(a), RAA may suffer from signal blockage issue with multiple differently orientated sULAs in the same plane.

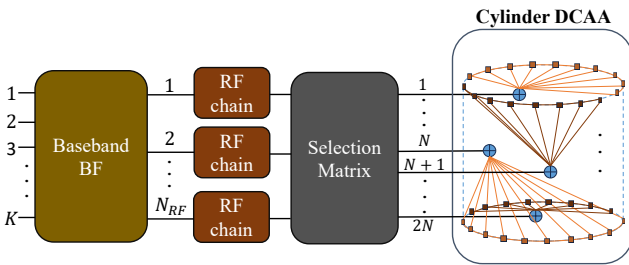


Fig. 2. The overall scheme of communication system with cylinder DCAA. $2N$ sub-arrays are selectively connected to N_{RF} RF chains through the selection matrix.

To address this problem, we propose a novel cylinder DCAA-based wireless communication system, as shown in Fig. 1(b) and Fig. 2. The proposed cylinder DCAA has N vertically stacked sUCAs and each sUCA is partitioned

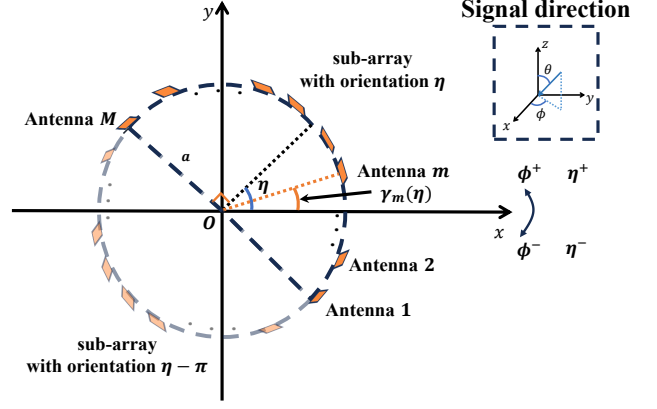


Fig. 3. An illustration of sUCA with $2M$ antenna elements partitioned into two sub-arrays, where M antenna elements are arranged into a uniform semi-circular architecture with orientation angle η or $\eta - \pi$ relative to the positive x axis and the m th antenna element in the sub-array has the orientation angle $\gamma_m(\eta)$ or $\gamma_m(\eta - \pi)$, respectively.

into two complementary directly-connected sub-arrays. To adaptively connect $2N$ sub-arrays to N_{RF} RF chains for further digital baseband processing, a *selection matrix* denoted by $\mathbf{S} \in \{0, 1\}^{N_{\text{RF}} \times 2N}$ which satisfies $\|\mathbf{S}\|_{i,:} = 1$ and $\|\mathbf{S}\|_{:,n} \leq 1$, $1 \leq i \leq N_{\text{RF}}$ and $1 \leq n \leq 2N$ is introduced. Through the selection matrix, the communication system with cylinder DCAA can serve K users with the number of RF chains being $N_{\text{RF}} \ll N$ without analog beamforming, thus decreasing hardware costs and complexity. In the following section, we will discuss the characteristics of sUCA, which is the basic component of cylinder DCAA.

III. SIMPLE UNIFORM CIRCULAR ARRAY

As illustrated in Fig. 3, a sUCA consists of $2M$ uniformly spaced directional antenna elements along a circular ring of radius a on the xOy plane. The sUCA is equally partitioned into two sub-arrays each consisting of M antenna elements, where the orientation angle η of a sub-array is defined as the orientation angle of the central antenna element relative to the reference positive x axis, and the m th element in the sub-array with orientation η has the orientation angle $\gamma_m(\eta)$, $m = 1, 2, \dots, M$. Since the response pattern of sUCA is the combination of response patterns of two complementary sub-arrays, in the following part, we will focus on the response pattern of a semi-circular-configured sub-array. The array's radius a is given by:

$$a = \frac{(M-1)\lambda}{2\pi} \approx \frac{M\lambda}{2\pi}, \quad M \gg 1, \quad (1)$$

where λ is the wavelength. The orientation angle of the m th antenna element $\gamma_m(\eta)$ relative to the positive x axis is given by:

$$\gamma_m(\eta) = \eta - \frac{\pi}{2} + \frac{\pi}{M-1}(m-1). \quad (2)$$

Thus, the three dimensional location vector of the m th antenna element is given by:

$$\mathbf{v}_m(\eta) = [a \cos \gamma_m(\eta), a \sin \gamma_m(\eta), 0]^T. \quad (3)$$

The uniform plane wave (UPW) signal that comes from azimuth angle ϕ and zenith angle θ is considered. Its direction vector is given by $\mathbf{k} = [\cos \phi \sin \theta, \sin \phi \sin \theta, \cos \theta]^T$. The projection of $\mathbf{v}_m(\eta)$ on \mathbf{k} is given by:

$$\begin{aligned} \mathbf{v}_m^T(\eta)\mathbf{k} &= a \sin \theta (\cos(\gamma_m(\eta)) \cos \phi + \sin(\gamma_m(\eta)) \sin \phi) \\ &= a \sin \theta \cos(\phi - \gamma_m(\eta)). \end{aligned} \quad (4)$$

Thus, the array response vector of a sub-array with orientation angle η for a UPW with (ϕ, θ) is given by:

$$\begin{aligned} \mathbf{a}(\eta, \phi, \theta) &= \left[e^{-j \frac{2\pi}{\lambda} a \sin \theta \cos(\xi_1(\eta))}, e^{-j \frac{2\pi}{\lambda} a \sin \theta \cos(\xi_2(\eta))}, \right. \\ &\quad \left. \dots, e^{-j \frac{2\pi}{\lambda} a \sin \theta \cos(\xi_M(\eta))} \right]^T \odot \mathbf{b}(\eta, \phi, \theta), \end{aligned} \quad (5)$$

where $\mathbf{b}(\eta, \phi, \theta)$ represents the element pattern vector, which is given by:

$$\mathbf{b}(\eta, \phi, \theta) = \left[\sqrt{G(\xi_1(\eta), \psi)}, \dots, \sqrt{G(\xi_M(\eta), \psi)} \right]^T, \quad (6)$$

where $G(\cdot)$ is the antenna element radiation pattern with $\xi_m(\eta) = \phi - \gamma_m(\eta)$ and $\psi = \theta - \frac{\pi}{2}$.

In order to align the sub-array's main lobe with its physical orientation angle η , a variable length antenna element delay line technology is introduced [21] to shift each antenna element's radiation phase. Since variable delay line technology employs passive delay lines with predefined delay values set via simple jumper configurations on the printed circuit board (PCB), the implementation will not introduce significant additional hardware costs and is relatively straightforward in terms of fabrication. As illustrated in Fig. 4, the delay line's length of the m th antenna element in a sub-array is given by l_m . Instead of fixed length antenna feeding where each antenna element has equal length delay line, i.e., $l_1 = l_2 = \dots = l_M$ and the adaptive phase shift is achieved through the phase shifter of each antenna element, the variable-length delay line in Fig. 4 will introduce different radiation phases for every antenna element. By carefully designing the length of every element's delay line, we can align the main lobe of the sub-array to the desired direction. Array factor $\text{AF}(\eta, \phi, \theta)$ of the sub-array with orientation η is given by:

$$\begin{aligned} \text{AF}(\eta, \phi, \theta) &= \mathbf{a}^T(\eta, \phi, \theta) \boldsymbol{\delta}(\eta, \theta) \\ &= \sum_{m=1}^M \sqrt{G(\xi_m(\eta), \psi)} e^{-j(\frac{2\pi}{\lambda} a \sin \theta \cos \xi_m(\eta) - \Delta \varphi_m(\eta, \theta))}, \end{aligned} \quad (7)$$

where $\boldsymbol{\delta}(\eta, \theta)$ is the phase shift vector achieved by the delay line, which is given by:

$$\boldsymbol{\delta}(\eta, \theta) = \left[e^{j \Delta \varphi_1(\eta, \theta)}, e^{j \Delta \varphi_2(\eta, \theta)}, \dots, e^{j \Delta \varphi_M(\eta, \theta)} \right]^T, \quad (8)$$

with $\Delta \varphi_m(\eta, \theta)$ being the phase shift of the m th antenna element introduced by the delay line. To simplify calculation, every antenna element's delay micro-strip line is considered as an ideal transmission line, thus the phase shift of the m th antenna element in the sub-array with orientation η is given by:

$$\Delta \varphi_m(\eta, \theta) = -\frac{2\pi}{\lambda} l_m(\eta, \theta). \quad (9)$$

Similar to the RAA architecture [18], we hope the main lobe of the sub-array with orientation η align with the direction $\phi = \eta$. Thus, the phase shift of the m th antenna element $\Delta \varphi_m(\eta, \theta)$ is given by:

$$\begin{aligned} \Delta \varphi_m(\eta, \theta) &= \frac{2\pi}{\lambda} a \sin \theta \cos(\eta - \gamma_m(\eta)) + 2k\pi \\ &= \frac{2\pi}{\lambda} a \sin \theta \sin\left(\frac{\pi}{M-1}(m-1)\right) + 2k\pi, \end{aligned} \quad (10)$$

where $k = 1, 2, \dots$. From (9) and (10), the delay line's length of the m th antenna element is given by:

$$\begin{aligned} l_m(\eta, \theta) &= \min_{k_m} \left[-a \sin \theta \sin\left(\frac{\pi}{M-1}(m-1)\right) + k_m \lambda \right] \\ \text{s.t. } &\begin{cases} l_m(\eta, \theta) > 0 \\ k_m = 1, 2, \dots, \end{cases} \end{aligned} \quad (11)$$

where k_m corresponds the integer k in (10) for the m th antenna element. Based on the fact that the link distance is much greater than the height difference between the transmitter and receiver, we only consider the signal comes around the xOy plane in the parameters design process, i.e., $\theta \approx \frac{\pi}{2}$. It is obvious that the m th and the $(M+1-m)$ th antenna element have the equal minimum length of the delay line and $l_m(\eta, \theta) = l_m$ is independent of the orientation angle η , such that the variable-length delay line design has good compliance with the principle of symmetry. Thus, the length of minimum delay line in (11) is reduced to:

$$l_m = -a \sin\left(\frac{\pi}{M-1}(m-1)\right) + k_m \lambda, \quad (12)$$

where the integer k_m that keeps the non-negativity of l_m is formulated by:

$$k_m = \left\lceil \frac{a}{\lambda} \sin\left(\frac{\pi}{M-1}(m-1)\right) \right\rceil. \quad (13)$$

Based on (12), the phase shift $\Delta \varphi_m(\eta, \theta) = \Delta \varphi_m$ in (10) and the phase shift vector $\boldsymbol{\delta}(\eta, \theta) = \boldsymbol{\delta}$ in (8) are independent of physical orientation of the sub-array.

With the variable length antenna delay line technology, array factor of the sub-array with orientation η is further expressed by:

$$\begin{aligned} \text{AF}(\eta, \phi, \theta) &= \sum_{m=1}^M \sqrt{G(\xi_m(\eta), \psi)} e^{-j \frac{2\pi}{\lambda} a \sin \theta (\cos \xi_m(\eta) - \cos(\eta - \gamma_m(\eta)))} \\ &= \sum_{m=1}^M \sqrt{G(\xi_m(\eta), \psi)} e^{j \frac{4\pi}{\lambda} a \sin \theta \sin\left(\frac{\phi + \eta - 2\gamma_m(\eta)}{2}\right) \sin\left(\frac{\phi - \eta}{2}\right)} \\ &= \sum_{m=1}^M \sqrt{G(\xi_m(\eta), \psi)} e^{j \frac{4\pi}{\lambda} a \sin \theta \cos\left(\frac{\phi - \eta}{2} - \frac{\pi}{M-1}(m-1)\right) \sin\left(\frac{\phi - \eta}{2}\right)} \end{aligned} \quad (14)$$

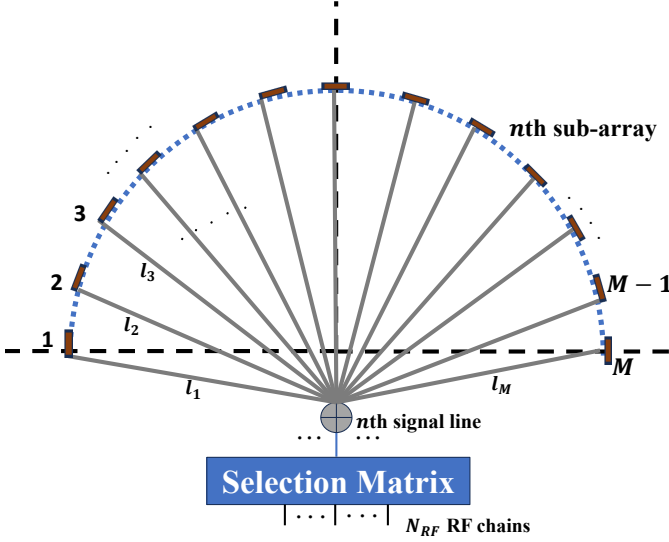


Fig. 4. The variable delay line technology. M antenna elements in a sub-array have different radiation phases based on carefully designed variable delay line.

With Jacobi-Anger expansion, the response can be further expressed by:

$$\begin{aligned}
 \text{AF}(\eta, \phi, \theta) &= \sum_{m=1}^M \sqrt{G(\xi_m(\eta), \psi)} \times \\
 &\sum_{n=-\infty}^{+\infty} j^n J_n \left(\frac{4\pi}{\lambda} a \sin \theta \sin \frac{\phi - \eta}{2} \right) e^{jn \frac{\phi - \eta}{2}} e^{-jn \frac{\pi(m-1)}{M-1}} \\
 &= \sum_{n=-\infty}^{+\infty} j^n e^{jn \frac{\phi - \eta}{2}} J_n \left(\frac{4\pi}{\lambda} a \sin \theta \sin \frac{\phi - \eta}{2} \right) \times \\
 &\sum_{m=1}^M \sqrt{G(\xi_m(\eta), \psi)} e^{-jn \frac{\pi(m-1)}{M-1}} \\
 &= \sum_{n=-\infty}^{+\infty} j^n e^{jn \frac{\phi - \eta}{2}} J_n \left(\frac{4\pi}{\lambda} a \sin \theta \sin \frac{\phi - \eta}{2} \right) S_n(\eta, \phi, \theta), \quad (15)
 \end{aligned}$$

where $J_n(\cdot)$ refers to the Bessel function of the first kind and $S_n(\eta, \phi)$ is given by:

$$S_n(\eta, \phi, \theta) = \sum_{m=1}^M \sqrt{G(\xi_m(\eta), \psi)} e^{-jn \frac{\pi(m-1)}{M-1}}. \quad (16)$$

Based on the characteristics of the Bessel function of the first kind, the position of the first valley point of $|\text{AF}(\eta, \phi, \theta)|$ mainly depends on the zeroth-order Bessel function $J_0(\cdot)$. To get an approximate but explicit expression of the distance $\phi_0 = |\phi_{\text{valley}} - \eta|$ between the first valley point ϕ_{valley} of $|\text{AF}(\eta, \phi, \theta)|$ relative to azimuth angle ϕ and the main lobe's direction η , the approximated value $\tilde{\phi}_0$ is modeled as the first zero point of $J_0 \left(\frac{4\pi}{\lambda} a \sin \theta \sin \frac{\phi}{2} \right) \Big|_{\theta=\frac{\pi}{2}}$. Thus, the approximation $\tilde{\phi}_0$ is given by:

$$\tilde{\phi}_0 = 2 \arcsin \left(\frac{3.83\lambda}{4\pi a} \right) = 2 \arcsin \left(\frac{3.83}{2M} \right). \quad (17)$$

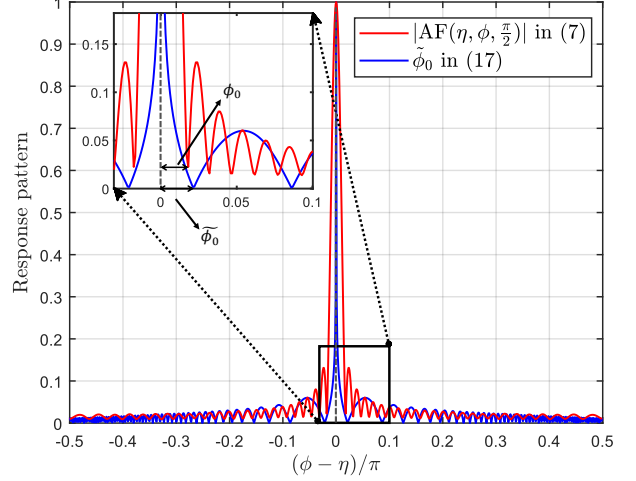


Fig. 5. Comparison of theoretical and approximated valley point of the uniform $|\text{AF}(\eta, \phi, \pi/2)|$ in (7) and (17) with $M = 64$ under carrier frequency $f_c = 47.2\text{GHz}$. Results show that the approximated $\tilde{\phi}_0$ is very close to the theoretical ϕ_0 .

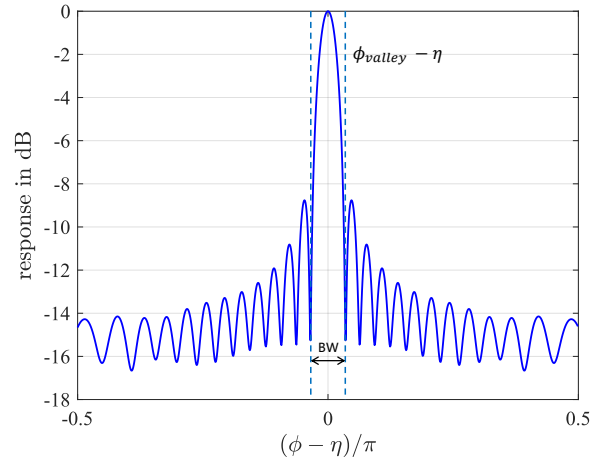


Fig. 6. Response pattern $|\text{AF}(\eta, \phi, \pi/2)|$ of the sub-array with orientation η and $M = 32$ in (7) with variable length delay line.

With $M \gg 1$ in XL-MIMO system, (17) is simplified to $\tilde{\phi}_0 \approx \frac{3.83}{M}$. As illustrated in Fig. 5, $\tilde{\phi}_0$ is very close to the exact ϕ_0 in (7), where antenna elements' radiation pattern $G(\xi, \psi)$ adopts the 3D 3GPP technical report [22] whose representation in dB is given by:

$$G_{\text{dB}}(\xi_m, \psi) = -\min \{ -(A_{\text{dB}}(\xi_m, \psi = 0) + A_{\text{dB}}(\xi_m = 0, \psi)), 30 \text{ dB} \} \quad (18a)$$

$$\begin{cases} A_{\text{dB}}(\xi_m, \psi = 0) = -\min \left[12 \left(\frac{\xi_m}{65^\circ} \right)^2, 30 \text{ dB} \right] \\ A_{\text{dB}}(\xi_m = 0, \psi) = -\min \left[12 \left(\frac{\psi}{65^\circ} \right)^2, 30 \text{ dB} \right] \end{cases} \quad (18b)$$

with $G_{\text{dB}}(\xi_m, \psi) = 10 \log_{10}(G(\xi_m, \psi))$ being the antenna gain expressed in dB.

Fig. 6 illustrates the response pattern $|AF(\eta, \phi, \pi/2)|$ given in (7) of a directly-connected sub-array given in Fig. 3, with $M = 32$ under central frequency $f_c = 47.2\text{GHz}$. The results reveal that the proposed directly-connected sub-array aligns its main beam lobe to its physical orientation, implying its advance performance in spatial resolution and interference suppression. Based on (7) and (15), we can derive *Theorem 1* that illustrates the characteristics of sub-array's response pattern.

Theorem 1: The maximum value of array factor $|AF(\eta, \phi, \theta)|$ given in (15) appears at angle set $(\phi, \theta) = (\eta, \frac{\pi}{2})$. The beam width of $|AF(\eta, \phi, \theta)|$ is given by $BW \approx 2\phi_0 = 4 \arcsin(\frac{3.83}{2M})$.

Proof: Please refer to Appendix A. ■

Theorem 1 reveals that sub-array can align the compact main beam lobe to the direction relative to its physical orientation η . For $M \gg 1$, the beam width is approximated as $BW \approx \frac{7.66}{M}$, which decreases with the number of antenna elements M in a sub-array.

IV. PROPOSED CYLINDER DCAA

In this section, based on the sUCA presented in Section III, a novel cylinder DCAA architecture is proposed.

A. Cylinder DCAA basic structure

As illustrated in Fig. 7, a cylinder DCAA is composed of $2N$ sub-arrays arranged by $2N \times M$ antenna elements, where each sub-array has M antenna elements, and every two sub-arrays that have complementary orientation angles, i.e., the difference of their orientation angles equals to π , are merged into a sUCA. Each sub-array has the antenna elements directly connected together through variable delay line technology without any digital or analog beamforming. Without loss of generality, a 3D Cartesian coordinate system is established, where the positive x axis is chosen as the reference direction for azimuth angle ϕ and sub-array's orientation η .

Since each sUCA is equally partitioned into two complementary sub-arrays, for sub-arrays in the n th sUCA, we use sub-array_n^+ and sub-array_n^- to denote the sub-array that has positive and negative orientation angle denoted by $\eta_n^+ > 0$ and $\eta_n^- < 0$ relative to the reference direction, respectively.

Since N sUCAs need to be arranged into a 3D layered structure, we define h as the distance between vertically adjacent sUCAs. Without loss of generality, we choose the positive z axis as the direction where a sUCA is stacked. Hence, the height of cylinder DCAA that has N sUCAs is given by $h_{\text{sum}} = (N-1)h$. Thus, a cylinder DCAA is characterized by the parameters $\{M, N, \{\eta_n^+\}, \{\eta_n^-\}, h_{\text{sum}}\}$.

B. Cylinder DCAA parameter design

To minimize interference between vertically adjacent sub-arrays, from the beamwidth BW given in *Theorem 1*, their orientations are designed so that one sub-array's main lobe locates at the vertically adjacent sub-array's valley point, i.e.,

$$\begin{aligned} \eta_n^+ &= 2n \arcsin\left(\frac{3.83}{2M}\right) \\ \eta_n^- &= \eta_n^+ - \pi = 2n \arcsin\left(\frac{3.83}{2M}\right) - \pi. \end{aligned} \quad (19)$$

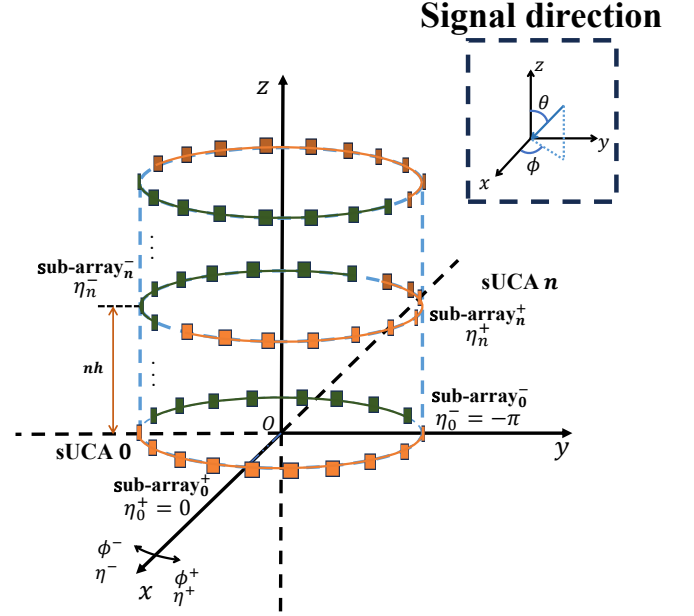


Fig. 7. Cylinder DCAA with N sUCAs with each of them consists of two complementary sub-arrays. sub-array_n^+ and sub-array_n^- has the orientation angle of η_n^+ and η_n^- relative to the positive x axis, respectively.

Based on the fact that the link distance is much greater than the height difference between the transmitter and receiver XL-MIMO, we obtain that $M \gg 1$ and $\theta = \frac{\pi}{2}$, thus orientation angle of the sub-array_n^+ is further given by $\eta_n^+ = n \times \frac{3.83}{M}$.

To cover the full-angle domain, the maximum orientation angle should satisfy $\eta_{N-1}^+ = \pi - \phi_0$. Thus, the number of sUCA that consists of two complementary sub-arrays is:

$$N = \left\lceil \frac{\pi M}{3.83} \right\rceil. \quad (20)$$

Some typical (M, N) sets are given by $(16, 13)$, $(32, 26)$, $(64, 52)$ and $(128, 104)$. For the sub-array_n^+ , the response vector is obtained by substituting η with η_n^+ in (5):

$$\begin{aligned} \mathbf{a}(\eta_n^+, \phi, \theta) &= \left[e^{-j \frac{2\pi}{\lambda} a \sin \theta \cos \xi_1(\eta_n^+)}, e^{-j \frac{2\pi}{\lambda} a \sin \theta \cos \xi_2(\eta_n^+)} \right. \\ &\quad \left. , \dots, e^{-j \frac{2\pi}{\lambda} a \sin \theta \cos \xi_M(\eta_n^+)} \right]^T \odot \mathbf{b}(\eta_n^+, \phi, \theta), \end{aligned} \quad (21)$$

where the antenna radiation pattern vector $\mathbf{b}(\eta_n^+, \phi, \theta)$ is obtained by substituting η with η_n^+ in (6):

$$\mathbf{b}(\eta_n^+, \phi, \theta) = \left[\sqrt{G(\xi_1(\eta_n^+), \psi)}, \dots, \sqrt{G(\xi_M(\eta_n^+), \psi)} \right]^T. \quad (22)$$

The response vector of sub-array_n^- is obtained by substituting η_n^+ in (21) and (22) with the complementary orientation angle $\eta_n^- = \eta_n^+ - \pi$ in (19).

The n th sUCA has the height of nh relative to the xOy plane, where we choose $h = \frac{\lambda}{2}$ to separate vertically adjacent sUCAs by half wavelength. Hence, the total height of the cylinder DCAA is given by $h_{\text{sum}} = \frac{(N-1)\lambda}{2}$.

The response pattern of cylinder DCAA with $M = 16$ directional antenna elements and $N = 13$ is shown in Fig. 8,

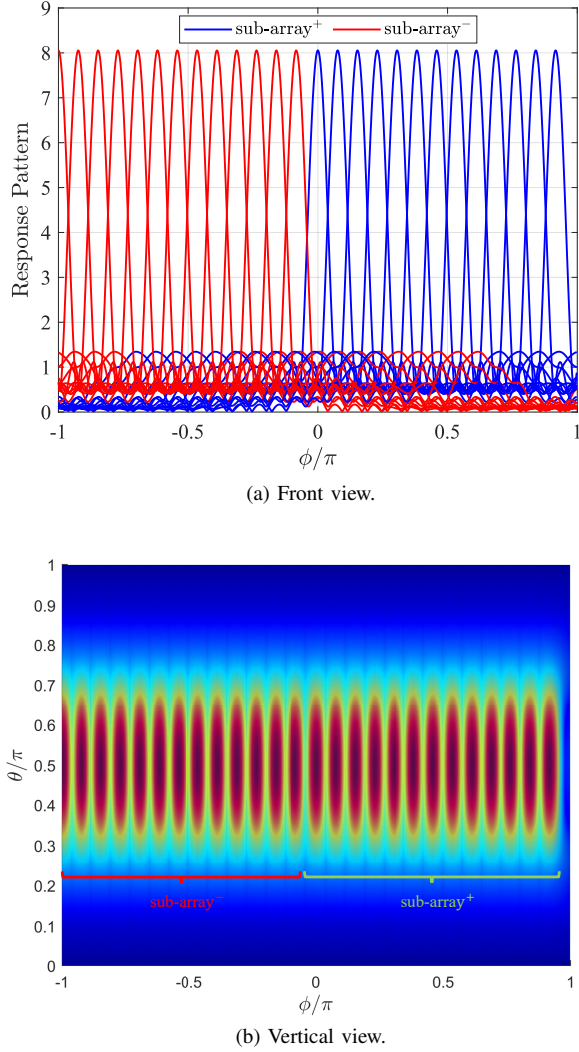


Fig. 8. Response pattern of cylinder DCAA with $M = 16$, $N = 13$. Cylinder DCAA achieves uniform spatial resolution with multiples sUCAs arranged with different physical orientations.

illustrating that the cylinder DCAA achieves uniform spatial resolution without relying on any front-end phase shifter, where sub-arrays⁺ uniformly cover the positive angle domain $\phi \in [0, \pi)$ and sub-arrays⁻ uniformly cover the negative angle domain $\phi \in [-\pi, 0)$. The design of orientation angle η_n^+ and η_n^- ensures that the sub-arrays will have as little interference as possible among vertically adjacent sub-arrays.

V. WIRELESS COMMUNICATION WITH CYLINDER DCAA

In this section, we consider wireless communication systems with the proposed cylinder DCAA and the benchmark cell sectoring system based on ULA with HBF.

A. The proposed cylinder DCAA

We first present the response matrix $\mathbf{A}(\phi, \theta) \in \mathbb{C}^{M \times 2N}$ of communication system with cylinder DCAA illustrated in Fig. 2. The response matrix is combined by 2 sub-matrices, i.e., $\mathbf{A}(\phi, \theta) = [\mathbf{A}^+(\phi, \theta), \mathbf{A}^-(\phi, \theta)]$, where $\mathbf{A}^+(\phi, \theta) \in \mathbb{C}^{M \times N}$ consists of the response vectors of N sub-arrays with relatively

positive orientation denoted by sub-arrays⁺ and $\mathbf{A}^-(\phi, \theta) \in \mathbb{C}^{M \times N}$ consists of the response vectors of N sub-arrays with relatively negative orientation denoted by sub-arrays⁻. From (21), the response matrix $\mathbf{A}(\phi, \theta)$ is given by:

$$\mathbf{A}(\phi, \theta) = \begin{bmatrix} \underbrace{[\mathbf{a}(\eta_0^+), \dots, \mathbf{a}(\eta_{N-1}^+)]}_{\triangleq \mathbf{A}^+(\phi, \theta)}, & \underbrace{[\mathbf{a}(\eta_0^-), \dots, \mathbf{a}(\eta_{N-1}^-)]}_{\triangleq \mathbf{A}^-(\phi, \theta)} \end{bmatrix}, \quad (23)$$

where $\mathbf{a}(\eta_n^+)$ stands for $\mathbf{a}(\eta_n^+, \phi, \theta)$ given in (21) and $\mathbf{a}(\eta_n^-)$ stands for $\mathbf{a}(\eta_n^-, \phi, \theta)$ derived by substituting η_n^+ with η_n^- . The resulting outputs of all $2N$ sub-arrays in N sUCAs are expressed by $\mathbf{r}(\phi, \theta) \in \mathbb{C}^{2N \times 1}$ which is given by:

$$\begin{aligned} \mathbf{r}(\phi, \theta) &= \mathbf{A}^T(\phi, \theta) \boldsymbol{\delta} \\ &= [\text{AF}(\eta_0^+, \phi, \theta), \dots, \text{AF}(\eta_{N-1}^+, \phi, \theta), \\ &\quad \text{AF}(\eta_0^-, \phi, \theta), \dots, \text{AF}(\eta_{N-1}^-, \phi, \theta)]^T, \end{aligned} \quad (24)$$

where $\text{AF}(\eta_n^+, \phi, \theta)$ and $\text{AF}(\eta_n^-, \phi, \theta)$ is the array factor of sub-array⁺ _{n} or sub-array⁻ _{n} given in (15) and $\boldsymbol{\delta}$ is the phase shift vector in (8) introduced by variable delay line and is irrelevant to physical orientation.

From the definition of *selection matrix* given in Section II, for a given RF chain tagged $i \in [1, N_{\text{RF}}]$, there always exists a sub-array tagged $n \in [1, 2N]$, such that $[\mathbf{S}]_{i,n} = 1$ and other elements in the row i being 0. We can further define a set Ω that illustrates N_{RF} chosen sub-arrays, which is given by:

$$\Omega = \{n : \|[\mathbf{S}]_{:,n}\| = 1\}, \quad (25)$$

where $i, n \in \mathbb{Z}_+$. In the following two sections, we will present SINR performance of the uplink and downlink communication system with the proposed cylinder DCAA.

1) *Uplink scenario*: For the uplink scenario of the proposed cylinder DCAA, the effective channel vector of the k th user $\mathbf{h}_{\text{UP},k} \in \mathbb{C}^{2N \times 1}$ is given by:

$$\mathbf{h}_{\text{UP},k} = \sum_{l=1}^{L_k} \alpha_{k,l} \mathbf{r}(\phi_{k,l}, \theta_{k,l}), \quad (26)$$

where L_k is the number of multipath components (MPCs) for the k th user and $\alpha_{k,l}$ is the complex attenuation parameter of the l th MPC for the k th user.

The additive Gaussian noise of each antenna element is given by matrix $\mathbf{Z} = [\mathbf{z}_1, \mathbf{z}_2, \dots, \mathbf{z}_{2N}]^T \in \mathbb{C}^{2N \times M}$, and $\mathbf{z}_n \sim \mathcal{CN}(0, \sigma^2 \mathbf{I}_M)$, $n = 1, 2, \dots, 2N$, where σ^2 is the noise power. For notational convenience, we can derive an equivalent additive noise vector $\mathbf{z}' \in \mathbb{C}^{2N \times 1}$ for $2N$ sub-arrays which is given by:

$$\mathbf{z}' = \mathbf{Z} \boldsymbol{\delta}. \quad (27)$$

Thereby $\mathbf{z}' \sim \mathcal{CN}(0, M\sigma^2 \mathbf{I}_{2N})$ is the equivalent sum noise vector over the M elements of the $2N$ sub-arrays. The resulting uplink signal for the k th user at the cylinder DCAA BS side is given by:

$$y_{\text{UP},k} = \underbrace{\mathbf{w}_k^H \mathbf{S} \mathbf{h}_{\text{UP},k}}_{k\text{th user's signal}} s_k + \underbrace{\mathbf{w}_k^H \mathbf{S} \sum_{i \neq k} \mathbf{h}_{\text{UP},i} s_i}_{\text{inter-user interference}} + \underbrace{\mathbf{w}_k^H \mathbf{S} \mathbf{z}'}_{\text{additive noise}}, \quad (28)$$

where $\mathbf{w}_k \in \mathbb{C}^{N_{\text{RF}} \times 1}$ is the baseband beamforming vector of the k th user, \mathbf{z}' is the equivalent sum noise vector given in (27), s_k is the information-bearing symbol of the k th user that satisfies $\mathbb{E}[|s_k|^2] = P_{\text{UP},k}$, where $P_{\text{UP},k}$ is the transmit power of the k th user. Hence, SINR of the k th user of cylinder DCAA is given by:

$$\text{SINR}_{\text{UP},k} = \frac{\bar{P}_{\text{UP},k} |\mathbf{w}_k^H \mathbf{S} \mathbf{h}_{\text{UP},k}|^2}{\sum_{i \neq k} \bar{P}_{\text{UP},i} |\mathbf{w}_k^H \mathbf{S} \mathbf{h}_{\text{UP},i}|^2 + M \|\mathbf{w}_k^H \mathbf{S}\|^2}, \quad (29)$$

where $\bar{P}_{\text{UP},k} = P_{\text{UP},k}/\sigma^2$ is the transmit SNR of the k th user. The achievable maximum sum rate of K users is given by:

$$R_{\text{sum,UP}}(\Omega) = \sum_{k=1}^K \log_2(1 + \text{SINR}_{\text{UP},k}). \quad (30)$$

We aim to maximize the sum rate $R_{\text{sum,UP}}(\Omega)$ of the cylinder DCAA for K users, and the optimization problem is given by:

$$\begin{aligned} \max_{\mathbf{S}, \mathbf{W}} \quad & R_{\text{sum,UP}}(\Omega) \\ \text{s.t.} \quad & \text{(C1): } \mathbf{S} \in \{0, 1\}^{N_{\text{RF}} \times 2N} \\ & \text{(C2): } \|\mathbf{S}\|_{i,:} = 1, \quad 1 \leq i \leq N_{\text{RF}} \\ & \text{(C3): } \|\mathbf{S}\|_{:,n} \leq 1, \quad 1 \leq n \leq 2N \\ & \text{(C4): } \Omega \text{ given in (25)} \\ & \text{(C5): } \mathbf{W} = [\mathbf{w}_1, \mathbf{w}_2, \dots, \mathbf{w}_K] \end{aligned} \quad (31)$$

where $\mathbf{W} \in \mathbb{C}^{N_{\text{RF}} \times K}$ is the baseband beamforming matrix consisting of K baseband beamforming vectors for all users. For any given selection matrix \mathbf{S} , the optimal receive beamforming is the linear minimum mean square error (MMSE) beamforming given by:

$$\mathbf{w}_k(\mathbf{S}) = \frac{\mathbf{C}_{\text{UP},k}^{-1}(\mathbf{S}) \mathbf{S} \mathbf{h}_{\text{UP},k}}{\|\mathbf{C}_{\text{UP},k}^{-1}(\mathbf{S}) \mathbf{S} \mathbf{h}_{\text{UP},k}\|}, \quad (32)$$

where $\mathbf{C}_{\text{UP},k}(\mathbf{S}) \in \mathbb{C}^{N_{\text{RF}} \times N_{\text{RF}}}$ is given by:

$$\mathbf{C}_{\text{UP},k}(\mathbf{S}) = \mathbf{S} \left(\sum_{i \neq k} P_{\text{UP},i} \mathbf{h}_{\text{UP},i} \mathbf{h}_{\text{UP},i}^H + M \sigma^2 \mathbf{I}_{2N} \right) \mathbf{S}^T. \quad (33)$$

Thus, (30) is reduced to:

$$R_{\text{sum,UP}}(\Omega) = \sum_{k=1}^K \log_2(1 + P_{\text{UP},k} (\mathbf{S} \mathbf{h}_k)^H \mathbf{C}_k^{-1}(\mathbf{S}) (\mathbf{S} \mathbf{h}_k)). \quad (34)$$

The greedy algorithm to find \mathbf{S} and \mathbf{W} in the uplink communication scenario is given by [19] in **Algorithm 1**.

2) *Downlink scenario*: For the downlink communication scenario with cylinder DCAA, the RF combiner of each sub-array needs to be replaced by a power splitter. The downlink transmit information-bearing symbol vector for K users is denoted by $\mathbf{s}_{\text{DL}} = [s_{\text{DL},1}, \dots, s_{\text{DL},K}]^T \in \mathbb{C}^{K \times 1}$, which satisfies $\mathbb{E}[\mathbf{s}_{\text{DL}} \mathbf{s}_{\text{DL}}^H] = \text{diag}([P_{\text{DL},1}, \dots, P_{\text{DL},K}])$, where $P_{\text{DL},k}$ denotes the transmit power for the k th user. The downlink baseband precoding matrix for K users is given by $\mathbf{W}_{\text{DL}} = [\mathbf{w}_{\text{DL},1}, \mathbf{w}_{\text{DL},2}, \dots, \mathbf{w}_{\text{DL},K}] \in \mathbb{C}^{N_{\text{RF}} \times K}$ with $\mathbf{w}_{\text{DL},k} \in \mathbb{C}^{N_{\text{RF}} \times 1}$ being the baseband precoding vector for the k th user. Thus, after going through the baseband processing

Algorithm 1 Greedy algorithm to obtain cylinder DCAA's selection matrix \mathbf{S} and baseband beamforming matrix \mathbf{W} in the uplink scenario.

-
- 1: Initialize $\Omega^0 = \emptyset$ and $n \in \mathcal{U}^0 = \{1, 2, \dots, 2N\}$
 - 2: **for** $i = 1 : N_{\text{RF}}$ **do**
 - 3: Calculate $n^i = \arg\max_{n \in \mathcal{U}^{i-1}} R_{\text{sum,UP}}(\Omega^{i-1} \cup n)$;
 - 4: Update $\Omega^i = \Omega^{i-1} \cup n^i$;
 - 5: Update $\mathcal{U}^i = \mathcal{U}^{i-1} \setminus n^i$;
 - 6: **end for**
 - 7: Obtain selection matrix \mathbf{S} based on $\Omega^{N_{\text{RF}}}$;
 - 8: Obtain baseband beamforming matrix \mathbf{W} based on \mathbf{S} .
 - 9: **Output**: \mathbf{S} , \mathbf{W} , and $R_{\text{sum,UP}}$
-

and the selection matrix $\mathbf{S} \in \mathbb{C}^{N_{\text{RF}} \times 2N}$, the transmitted signal vector $\mathbf{x}_{\text{DL}} \in \mathbb{C}^{2N \times 1}$ is given by:

$$\mathbf{x}_{\text{DL}} = \sqrt{\frac{1}{M}} \mathbf{S}^T \mathbf{W}_{\text{DL}} \mathbf{s}_{\text{DL}} = \sqrt{\frac{1}{M}} \mathbf{S}^T \sum_{k=1}^K \mathbf{w}_{\text{DL},k} s_{\text{DL},k}, \quad (35)$$

and the factor $\sqrt{1/M}$ is introduced by the power splitter for the M antenna elements in a sub-array. The downlink effective channel matrix for K users is denoted by $\mathbf{H}_{\text{DL}} = [\mathbf{h}_{\text{DL},1}, \mathbf{h}_{\text{DL},2}, \dots, \mathbf{h}_{\text{DL},K}]^T \in \mathbb{C}^{K \times 2N}$, where $\mathbf{h}_{\text{DL},k}$ is the downlink effective channel for the k th user:

$$\mathbf{h}_{\text{DL},k} = \sum_{l=1}^{L_k} \alpha_{k,l} \mathbf{r}(\phi_{k,l}, \theta_{k,l}). \quad (36)$$

Thus, after the transmitted signal vector given in (35) passing through the effective channel, the received signal vector $\mathbf{y}_{\text{DL}} = [y_{\text{DL},1}, y_{\text{DL},2}, \dots, y_{\text{DL},K}]^T \in \mathbb{C}^{K \times 1}$ of K users is given by:

$$\begin{aligned} \mathbf{y}_{\text{DL}} &= \mathbf{H}_{\text{DL}} \mathbf{x}_{\text{DL}} + \mathbf{z}_{\text{DL}} \\ &= \sqrt{\frac{1}{M}} \mathbf{H}_{\text{DL}} \mathbf{S}^T \sum_{k=1}^K \mathbf{w}_{\text{DL},k} s_{\text{DL},k} + \mathbf{z}_{\text{DL}}, \end{aligned} \quad (37)$$

where $\mathbf{z}_{\text{DL}} = [z_1, z_2, \dots, z_K]^T \sim \mathcal{CN}(0, \sigma^2 \mathbf{I}_K)$ is the noise vector of K users. The signal received by the k th user is given by:

$$\begin{aligned} y_{\text{DL},k} &= \mathbf{h}_{\text{DL},k}^T \mathbf{x}_{\text{DL}} + z_k \\ &= \sqrt{\frac{1}{M}} \mathbf{h}_{\text{DL},k}^T \left(\mathbf{S}^T \sum_{i=1}^K \mathbf{w}_{\text{DL},i} s_{\text{DL},i} \right) + z_k \\ &= \underbrace{\sqrt{\frac{1}{M}} \mathbf{h}_{\text{DL},k}^T \mathbf{S}^T \mathbf{w}_{\text{DL},k} s_{\text{DL},k}}_{\text{kth user's signal}} + \\ &\quad \underbrace{\sqrt{\frac{1}{M}} \mathbf{h}_{\text{DL},k}^T \mathbf{S}^T \left(\sum_{i \neq k} \mathbf{w}_{\text{DL},i} s_{\text{DL},i} \right)}_{\text{inter-user interference}} + z_k \end{aligned} \quad (38)$$

Based on (38), the SINR of the cylinder DCAA at downlink scenario is given by:

$$\text{SINR}_{\text{DL},k} = \frac{\frac{1}{M} P_{\text{DL},k} |\mathbf{h}_{\text{DL},k}^T \mathbf{S}^T \mathbf{w}_{\text{DL},k}|^2}{\frac{1}{M} \sum_{i \neq k} P_{\text{DL},i} |\mathbf{h}_{\text{DL},k}^T \mathbf{S}^T \mathbf{w}_{\text{DL},i}|^2 + \sigma^2}. \quad (39)$$

Thus, the achievable maximum sum rate for downlink scenario of cylinder DCAA is given by:

$$R_{\text{sum,DL}} = \sum_{k=1}^K \log_2(1 + \text{SINR}_{\text{DL},k}). \quad (40)$$

Specifically, from the uplink-downlink duality, for a given selection matrix \mathbf{S} , the optimal baseband transmit precoding is the MMSE precoding obtained from the dual uplink channels $\mathbf{H}_{\text{d-UP}} = \mathbf{H}_{\text{DL}}^H = [\mathbf{h}_{\text{DL},1}^*, \mathbf{h}_{\text{DL},2}^*, \dots, \mathbf{h}_{\text{DL},K}^*] \in \mathbb{C}^{2N \times K}$ [23]. And with appropriate power allocation strategy, the same SINR and achievable maximum sum rate can be met at the downlink channel and its dual uplink channel with the same summarized transmit power from BS and user equipments (UEs), respectively. $\mathbf{w}_{\text{DL},k}$ for the k th user in (38) is given by:

$$\mathbf{w}_{\text{DL},k}(\mathbf{S}, \mathbf{p}) = \frac{\mathbf{C}_{\text{DL},k}^{-1}(\mathbf{S}, \mathbf{p}) \mathbf{S} \mathbf{h}_{\text{DL},k}^*}{\|\mathbf{C}_{\text{DL},k}^{-1}(\mathbf{S}, \mathbf{p}) \mathbf{S} \mathbf{h}_{\text{DL},k}^*\|} \quad (41)$$

where $\mathbf{p} = [P_{\text{DL},1}, \dots, P_{\text{DL},K}]^T \in \mathbb{R}^{K \times 1}$ and $\mathbf{C}_{\text{DL},k}(\mathbf{S}, \mathbf{p}) \in \mathbb{C}^{N_{\text{RF}} \times N_{\text{RF}}}$ is given by:

$$\mathbf{C}_{\text{DL},k}(\mathbf{S}, \mathbf{p}) = \mathbf{S} \left(\sum_{i \neq k} P_{\text{DL},i} \mathbf{h}_{\text{DL},i}^* \mathbf{h}_{\text{DL},i}^T + M\sigma^2 \mathbf{I}_{2N} \right) \mathbf{S}^T. \quad (42)$$

We aim to maximize the downlink achievable sum rate $R_{\text{sum,DL}}$ given in (40) by adjusting *selection matrix* \mathbf{S} , baseband precoding matrix \mathbf{W}_{DL} and power allocation vector \mathbf{p} given in (44). Thus, the proposed optimization problem is given by:

$$\begin{aligned} \max_{\mathbf{S}, \mathbf{W}_{\text{DL}}, \mathbf{p}} \quad & R_{\text{sum,DL}} \\ \text{s.t.} \quad & (\text{C1}) - (\text{C3}) \text{ in (31)} \\ & (\text{D1}) \quad \mathbf{p}^T \mathbf{1}_{K \times 1} = P_{\text{DL}}, \end{aligned} \quad (43)$$

where P_{DL} is the summarized transmit power in the downlink communication and $\frac{P_{\text{DL}}}{K\sigma^2}$ is defined as the average transmit SNR. However, owing to the binary constraints in *selection matrix* \mathbf{S} and the tight coupling between \mathbf{S} , \mathbf{W}_{DL} and \mathbf{p} , problem (43) is difficult to be solved. Therefore, an iterative step-by-step optimization method for \mathbf{S} , \mathbf{W}_{DL} and \mathbf{p} is developed. For each iteration, \mathbf{S} is updated firstly using the greedy algorithm described in **Algorithm 1** with $\mathbf{H}_{\text{d-UP}}$. Then, \mathbf{p} and \mathbf{W}_{DL} w.r.t. \mathbf{S} are optimized using the classic iterative waterfilling method [24]. This process is repeated until convergence or meeting the maximum times of iterations. With waterfilling power allocation, the k th entry of \mathbf{p} is given by:

$$P_{\text{DL},k} \approx \max \left(\mu - \frac{Z_k}{|\mathbf{h}_{\text{DL},k}^T \mathbf{S}^T \mathbf{w}_{\text{DL},k}|^2}, 0 \right), \quad (44)$$

where Z_k is equivalent interference-plus-noise power which is given by:

$$Z_k = \sum_{j \neq k} P_{\text{DL},j} |\mathbf{h}_{\text{DL},k}^T \mathbf{S}^T \mathbf{w}_{\text{DL},j}|^2 + M\sigma^2, \quad (45)$$

and μ is the water level given by:

$$\mu = \frac{P_{\text{DL}}}{K} + \frac{1}{K} \sum_{k=1}^K \frac{Z_k}{|\mathbf{h}_{\text{DL},k}^T \mathbf{S}^T \mathbf{w}_{\text{DL},k}|^2}. \quad (46)$$

While iteratively updating \mathbf{S} based on the updated \mathbf{p} with **Algorithm 1** ensures accuracy, its computational complexity is over $\mathcal{O}(NN_{\text{RF}} \log(\frac{1}{\varepsilon_{\text{th}}}))$, where ε_{th} is the convergence threshold. The complexity is intolerable for instant communication considering channel coherency. To address this challenge, we propose a simplification where \mathbf{S} is updated only once during the initialization phase with uniform power allocation, i.e., $P_{\text{DL},k} = \frac{P_{\text{DL}}}{K}$, $k = 1, 2, \dots, K$. This trade-off between computational efficiency and accuracy is analyzed in Section VI-B, where it is demonstrated that the proposed method achieves a substantial reduction in computational complexity with only a little compromising of performance. Finally, the proposed downlink optimization algorithm is given by **Algorithm 2**.

Algorithm 2 Algorithm to obtain cylinder DCAA's *selection matrix* \mathbf{S} , baseband beamforming matrix \mathbf{W}_{DL} and power allocation vector \mathbf{p} in the downlink communication.

- 1: **Input:** Maximum iteration times T_{max} , convergence threshold ε_{th} , downlink effective channel \mathbf{H}_{DL} and summarized power P_{DL} ;
- 2: **Initialize:** $\mathbf{p}^{(0)} = \frac{P_{\text{DL}}}{K} \mathbf{1}_{K \times 1}$, $t = 0$;
- 3: Obtain \mathbf{S} , $\mathbf{W}_{\text{DL}}^{(0)}$ from **Algorithm 1**;
- 4: **repeat**
- 5: Update $t \leftarrow t + 1$;
- 6: Obtain $\mathbf{W}_{\text{DL}}^{(t)}$ from (41);
- 7: Obtain $\mathbf{p}^{(t)}$ from (44);
- 8: **if** $t \geq T_{\text{max}}$ **then**
- 9: **break**;
- 10: **end if**
- 11: **until** Convergence: $(\|\mathbf{p}^{(t)} - \mathbf{p}^{(t-1)}\|)^T \mathbf{1}_{K \times 1} < \varepsilon_{\text{th}}$
- 12: Calculate $\text{SINR}_{\text{DL},i}$, $i = 1, 2, \dots, K$ from (39);
- 13: **Output:** \mathbf{S} , $\mathbf{W}_{\text{DL}}^{(t)}$, $\mathbf{p}^{(t)}$, and $R_{\text{sum,DL}}$;

B. The benchmark: ULA with HBF structure

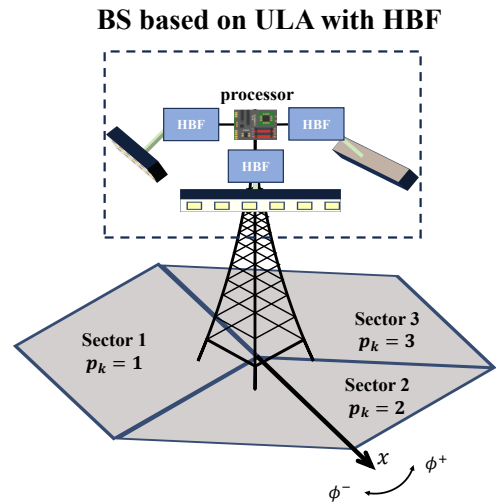


Fig. 9. The cell sectoring communication system where BS is equipped with ULA and uses HBF to achieve beam steering.

As illustrated in Fig. 9, we consider a widely implemented cell sectoring system based on ULA in 3GPP technical report

[22] with classic HBF as the benchmark. The cell sectoring system based on ULA with HBF is operated by dividing the cell into 3 sectors, and each covers an angle interval of 120° . The BS aligns a ULA with DFT codebook to serve users in the specific sector. Let $p_k \in \{1, 2, 3\}$ refers to the sector number of the k th user determined by the AoA ϕ_k which is defined as:

$$p_k = \begin{cases} 1 & (-\pi < \phi_k \leq -\frac{\pi}{3}) \\ 2 & (-\frac{\pi}{3} < \phi_k \leq \frac{\pi}{3}) \\ 3 & (\frac{\pi}{3} < \phi_k \leq \pi). \end{cases} \quad (47)$$

The response vector of the ULA that serves the sector p_k is given by:

$$\mathbf{a}_{\text{ULA}}(p_k, \phi) = \sqrt{G\left(\xi(p_k), \frac{\pi}{2}\right)} \left[1, e^{-j\pi \sin \xi(p_k)}, \dots, e^{-j\pi(M-1) \sin \xi(p_k)}\right]^T, \quad (48)$$

where the relative azimuth angle $\xi(p_k) = \phi - (p_k - 2)\frac{2\pi}{3}$. The effective channel of the k th user is given by:

$$\mathbf{h}_{\text{UP,ULA},k} = \sum_{l=1}^{L_k} \alpha_{k,l} \mathbf{a}_{\text{ULA}}(p_k, \phi_{k,l}), \quad (49)$$

where L_k is the number of paths of the k th user. The DFT codebook analog beamforming matrix $\mathbf{F} \in \mathbb{C}^{N_{\text{RF}} \times M}$ is given by:

$$\mathbf{F} = \mathbf{\Xi} \mathbf{U}, \quad (50)$$

where $\mathbf{U} = [\mathbf{u}_{l,m}] \in \mathbb{C}^{M \times M}$, $0 \leq l, m \leq M-1$ is the DFT matrix with $u_{l,m} = \exp(-j2\pi \frac{lm}{M})/\sqrt{M}$ and $\mathbf{\Xi} = (\mathbf{n}_1, \mathbf{n}_2, \dots, \mathbf{n}_{N_{\text{RF}}})^T$ is the digital selection matrix and the vector \mathbf{n}_i , $1 \leq i \leq N_{\text{RF}}$ has only one element being 1 and zero elsewhere. Given the substantial angular separation between different sectors and the deployment of directional antenna elements, the inter-sector interference is considered negligible compared to the intra-sector interference. Thus, the received signal solely focused on the intra-sector inter-user interference is given by:

$$y_{\text{UP,ULA},k} = \mathbf{w}_{\text{ULA},k}^H \mathbf{F} \left(\sum_{\substack{i=1 \\ p_i=p_k}}^K \mathbf{h}_{\text{UP,ULA},i} s_i + \mathbf{z} \right), \quad (51)$$

where $\mathbf{z} \sim \mathcal{CN}(0, \sigma^2 \mathbf{I}_M)$ is the additive noise and $\mathbf{w}_{\text{ULA},k}$ is the digital MMSE baseband beamforming vector which is given by:

$$\mathbf{w}_{\text{ULA},k} = P_{\text{UP},k} \mathbf{C}_{\text{ULA},k}^{-1}(\mathbf{F}) \mathbf{F} \mathbf{h}_{\text{UP,ULA},k}. \quad (52)$$

where $\mathbf{C}_{\text{ULA},k}(\mathbf{F}) \in \mathbb{C}^{N_{\text{RF}} \times N_{\text{RF}}}$ is given by:

$$\begin{aligned} \mathbf{C}_{\text{ULA},k}(\mathbf{F}) &= \sum_{\substack{i \neq k \\ p_i=p_k}} P_{\text{UP},i} (\mathbf{F} \mathbf{h}_{\text{UP,ULA},i}) (\mathbf{F} \mathbf{h}_{\text{UP,ULA},i})^H + \mathbf{F} \mathbf{F}^H \sigma^2 \\ &= \mathbf{F} \left(\sum_{\substack{i \neq k \\ p_i=p_k}} P_{\text{UP},i} \mathbf{h}_{\text{UP,ULA},i} \mathbf{h}_{\text{UP,ULA},i}^H + \sigma^2 \mathbf{I}_M \right) \mathbf{F}^H. \end{aligned} \quad (53)$$

Optimization process of digital selection matrix $\mathbf{\Xi}$ is given in [25]. Thus, SINR of the k th user in the cell sectoring system based on ULA with HBF is given by:

$$\begin{aligned} \text{SINR}_{\text{UP,ULA},k} &= \frac{P_{\text{UP},k} \left| \mathbf{w}_{\text{ULA},k}^H \mathbf{F} \mathbf{h}_{\text{UP,ULA},k} \right|^2}{\sum_{\substack{i \neq k \\ p_i=p_k}} P_{\text{UP},i} \left| \mathbf{w}_{\text{ULA},k}^H \mathbf{F} \mathbf{h}_{\text{UP,ULA},i} \right|^2 + \sigma^2 \|\mathbf{F}^H \mathbf{w}_{\text{ULA},k}\|^2}. \end{aligned} \quad (54)$$

Therefore, the achievable maximum sum rate of the benchmark system in the uplink communication scenario is given by:

$$R_{\text{sum,UP,ULA}} = \sum_{k=1}^K \log_2 (1 + \text{SINR}_{\text{UP,ULA},k}). \quad (55)$$

Similarly, for cell sectoring system based on ULA with HBF in the downlink scenario, the k th user's received signal is given by:

$$y_{\text{DL,ULA},k} = \sum_{\substack{i=1 \\ p_i=p_k}}^K \mathbf{h}_{\text{DL,ULA},k}^T \mathbf{F}^H \mathbf{w}_{\text{DL,ULA},i} s_i + z_k, \quad (56)$$

where $\mathbf{h}_{\text{DL,ULA},k} \in \mathbb{C}^{M \times 1}$ is the downlink effective channel for the k th user at sector denoted by p_k , $\mathbf{w}_{\text{DL,ULA},i} \in \mathbb{C}^{N_{\text{RF}} \times 1}$ is the transmit MMSE baseband beamforming vector of the i th user obtained from uplink-downlink duality [26] and the power splitting factor $\sqrt{1/M}$ is implied in the analog beamforming matrix \mathbf{F} . Thus, the SINR of the cell sectoring based on ULA with HBF is given by:

$$\begin{aligned} \text{SINR}_{\text{DL,ULA},k} &= \frac{P_{\text{DL},k} \left| \mathbf{h}_{\text{DL,ULA},k}^T \mathbf{F}^H \mathbf{w}_{\text{DL,ULA},k} \right|^2}{\sum_{\substack{i \neq k \\ p_i=p_k}} P_{\text{DL},i} \left| \mathbf{h}_{\text{DL,ULA},k}^T \mathbf{F}^H \mathbf{w}_{\text{DL,ULA},i} \right|^2 + \sigma^2}, \end{aligned} \quad (57)$$

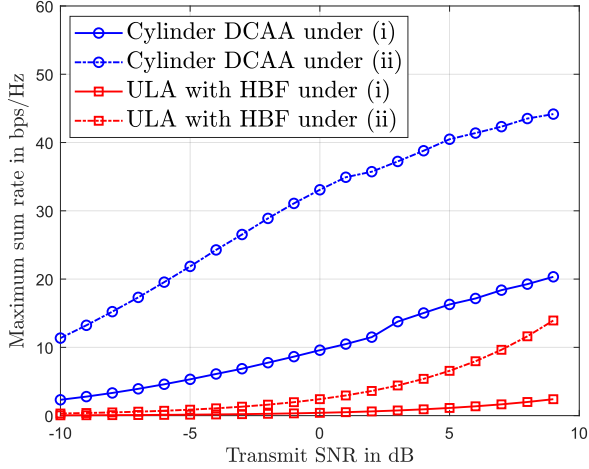
and the achievable maximum downlink sum rate of cell sectoring based on ULA with HBF is given by:

$$R_{\text{sum,DL,ULA}} = \sum_{k=1}^K \log_2 (1 + \text{SINR}_{\text{DL,ULA},k}). \quad (58)$$

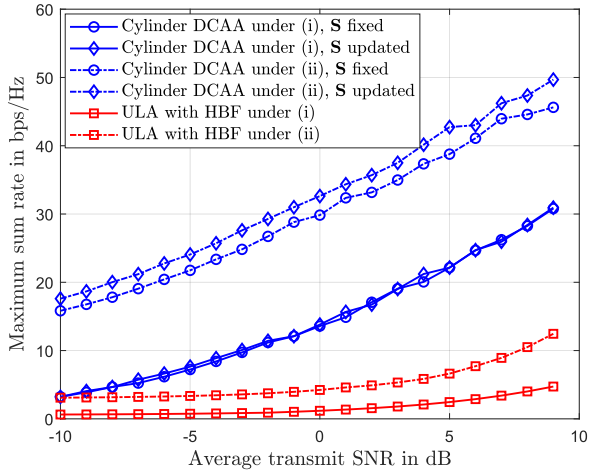
VI. SIMULATION AND NUMERICAL RESULTS

A. Uplink and downlink sum rate performance of cylinder DCAA

In this part, we present simulation results of the uplink and downlink maximum sum rate performance of the communication system with cylinder DCAA and compare it with the benchmark cell sectoring system based on ULA with HBF. Here we choose two typical communication scenarios: (i) normal connectivity with 10 users and (ii) dense connectivity with 30 users in a cell, detailed parameters are given in Table I. Wireless channel generation parameters for the simulation are shown in Table II. As illustrated in Fig. 10(a), for the uplink scenario, communication system with cylinder DCAA demonstrates superior maximum sum rate performance compared to cell sectoring system based on ULA with HBF, and the performance advantage is evident under both scenario (i)



(a) Uplink communication



(b) Downlink communication

Fig. 10. Uplink and downlink maximum sum rate performance comparison of the communication system with cylinder DCAA and the cell sectoring system based on ULA with HBF under 2 scenarios. The communication system with cylinder DCAA achieves higher maximum sum rate performance with same transmit SNR, especially in scenario (ii).

TABLE I
SIMULATION SCENARIOS.

Scenario	M : antennas per sub-array or ULA	N_{RF} : RF chains	K : users
(i) normal connectivity	64	10	10
(ii) dense connectivity	128	30	30
Antenna pattern: 3GPP directional antenna [22]			

and (ii), given the same transmit SNR at the user terminal. As illustrated in Fig. 10(b), with the same average transmit SNR denoted by $\frac{P_{\text{DL}}}{K\sigma^2}$ at BS side, cylinder DCAA still achieves superior maximum sum rate in the downlink communication than the cell sectoring system based on ULA with HBF, thanks to its uniform spatial resolution and the enhanced beamforming gain facilitated by the cylinder DCAA architecture. The satisfying simulation results imply that the proposed cylinder

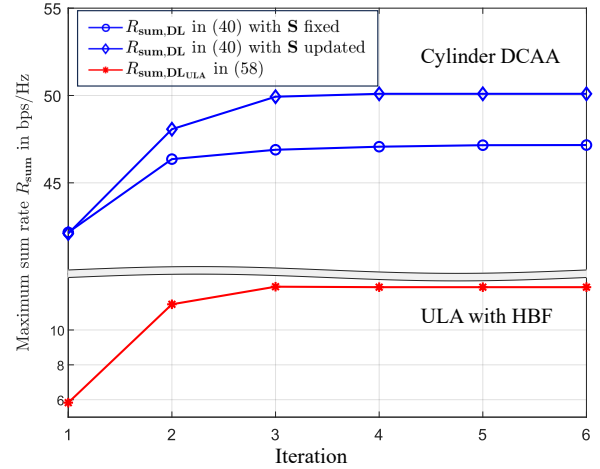


Fig. 11. Convergence of **Algorithm 2** for cylinder DCAA and ULA with HBF at the dense connectivity scenario, where $M = 128$, $K = N_{\text{RF}} = 30$ and $\varepsilon_{\text{th}} = 0.1$ under average transmit SNR being 9 dB.

DCAA is a potential cost-efficient solution for the high dense connectivity in the future 6G networks.

B. Effectiveness and convergence of the proposed Algorithm 2

As illustrated in Fig. 10(b), updating \mathbf{S} provides similar performance under scenario (i) and only 8.2% performance improvement compared with the fixed \mathbf{S} method given in **Algorithm 2** under scenario (ii). Therefore, by updating \mathbf{S} only once, we can achieve significantly lower computational complexity $\mathcal{O}(\log(\frac{1}{\varepsilon_{\text{th}}}))$ for the iteration process while maintaining satisfactory performance. This trade-off makes the single-update scheme a more practical choice for implementation.

Fig. 11 illustrates the convergence behavior of the proposed **Algorithm 2** for the proposed cylinder DCAA in scenario (ii) under average transmit SNR being 9 dB. Similarly, for cell sectoring system based on ULA with HBF, **Algorithm 2** is adapted to adjust DFT-based HBF matrix \mathbf{F} , baseband beamforming matrix $\mathbf{W}_{\text{DL,ULA}}$ and power allocation vector \mathbf{p} for larger maximum sum rate. We define the convergence threshold being $\varepsilon_{\text{th}} = 0.01$ for the power allocation vector \mathbf{p} . As illustrated in Fig. 11, the proposed **Algorithm 2** converges within 6 iterations for both cylinder DCAA and ULA with HBF. These results jointly validate the effectiveness and convergence of the proposed optimization algorithm.

C. Cost-efficiency and sensitivity analysis

In contrast to the cell sectoring system based on ULA with HBF that requires $3N_{\text{RF}}M$ phase shifters, the cylinder DCAA only needs $N_{\text{RF}}N$ single port double throw (SPDT) RF switches to achieve flexible beam steering, though at the expenditure of more antenna elements arranged in the array. For a system satisfying scenario (ii) discussed in Section VI-A that works under frequency 37 GHz, we assume a mmWave communication systems that employs the TPG2102 5-bits phase shifter and the TGS4302 SPDT RF switch. From the

TABLE II
SIMULATION PARAMETERS IN 3GPP INDOOR-OFFICE NLOS SCENARIO [22].

Parameter	Symbol	Definition / Value
Number of users	K	10 and 30
Number of RF chains	N_{RF}	10 and 30
LoS azimuth angle of the k th user	ϕ_k	$\phi_k \sim \mathcal{U}(-\pi, \pi)$ ($k = 1, 2, \dots, K$)
LoS zenith angle of the k th user	θ_k	$\theta_k = \pi/2$ ($k = 1, 2, \dots, K$)
Carrier central frequency	f_c	47.2GHz
Number of paths of the k th user	L_k	$L_k = N_c \times N_r$, $N_c = 19, N_r = 20$
Cluster delay	τ_{n_c}	$\tau_{n_c} = \text{sort}(\tau'_{n_c} - \min(\tau'_{n_c})), \tau'_{n_c} = -r_\tau \text{DS} \log(X_n)$ ($n_c = 1, 2, \dots, N_c$) $\text{lgDS} \sim \mathcal{N}(-7.173 - 0.28 \log_{10}(1 + f_c), (0.10 \log_{10}(1 + f_c) + 0.055)^2)$, $\text{lgDS} = \log_{10}(\text{DS}/1\text{s})$, $X_n \sim \mathcal{U}(0, 1)$, $r_\tau = 3$
Cluster power	P_{n_c}	$P_{n_c} = P'_{n_c} / \sum_{n_c=1}^{N_c} P'_{n_c}$, $P'_{n_c} = \exp(-\tau_{n_c}(r_\tau - 1)/(r_\tau \text{DS})) 10^{-Z_n/10}$ $Z_n \sim \mathcal{N}(0, 3^2)$, ($n_c = 1, 2, \dots, N_c$)
Azimuth angle spread	ASA	$\text{lgASA} \sim \mathcal{N}(1.863 - 0.11 \log_{10}(1 + f_c), (0.12 \log_{10}(1 + f_c) + 0.059)^2)$, $\text{lgASA} = \log_{10}(\text{ASA}/1^\circ)$
zenith angle spread	EAS	$\text{lgEAS} \sim \mathcal{N}(1.387 - 0.15 \log_{10}(1 + f_c), (-0.09 \log_{10}(1 + f_c) + 0.746)^2)$, $\text{lgEAS} = \log_{10}(\text{EAS}/1^\circ)$
Cluster azimuth angle	ϕ_{n_c}	$\phi_{n_c} = X_n \phi'_{n_c} + Y_n + \phi_k$, $X_n \in \{-1, 1\}$, $Y_n \sim \mathcal{N}(0, (\text{ASA}/7)^2)$ $\phi'_{n_c} = 2(\text{ASA}/1.4) \sqrt{-\log(P_{n_c}/\max(P_{n_c}))}/C_\phi$, $C_\phi = 1.273$
Cluster zenith angle	θ_{n_c}	$\theta_{n_c} = X_n \theta'_{n_c} + Y_n + \theta_k$, $X_n \in \{-1, 1\}$, $Y_n \sim \mathcal{N}(0, (\text{EAS}/7)^2)$ $\theta'_{n_c} = -\text{EAS} \log((P_{n_c}/\max(P_{n_c}))/C_\theta)/C_\theta$, $C_\theta = 1.184$
Ray power in cluster n_c	$P_{n_c,n}$	$P_{n_c,n} = P_{n_c} \times P'_{n_c,n} / \sum_{n=1}^N P'_{n_c,n}$ $P'_{n_c,n} = \exp(-\sqrt{2}\alpha_{\text{ASA}}/11) \exp(-\sqrt{2}\alpha_{\text{EAS}}/9)$, $\alpha_{\text{ASA}}, \alpha_{\text{EAS}} \sim \mathcal{U}(-2, 2)$
Ray azimuth angle in cluster n_c	$\phi_{n_c,n}$	$\phi_{n_c,n} = \phi_{n_c} + c_{\text{ASA}}\alpha_n$, $\alpha_n \sim \mathcal{U}(-2, 2)$
Ray zenith angle in cluster n_c	$\theta_{n_c,n}$	$\theta_{n_c,n} = \theta_{n_c} + c_{\text{EAS}}\alpha_n$, $\alpha_n \sim \mathcal{U}(-2, 2)$
Ray complex attenuation factor in cluster n_c	$\alpha_{n_c,n}$	$\alpha_{n_c,n} = \sqrt{P_{n_c,n}} \exp(j\Phi)$, $\Phi \sim \mathcal{U}(-\pi, \pi)$

manufacture's quotation, the detailed prices of the above basic hardware components are given in Table III.

TABLE III
HARDWARE COMPONENTS QUOTATION FOR MMWAVE COMMUNICATION.

carrier frequency $f_c = 37$ GHz		
Component	Symbol	Quotation in dollar
Antenna elements	c_{An}	0.01
TPG2102 5-bits phase shifter	c_{PS}	131.2 [8]
TGS4302 RF switch	c_{SW}	28.62 [9]

Accordingly, the primary hardware expenditures for the cylinder DCAA and cell sectoring based on ULA with HBF is given in Table IV. The results in Table IV demonstrates

TABLE IV
HARDWARE COSTS FOR TWO COMMUNICATION SYSTEMS.

$M = 128, K = N_{\text{RF}} = 30$		
System	Expression	Numerical results in dollar
Cylinder DCAA	$c_{\text{cyl}} = 2NM c_{\text{An}} + N_{\text{RF}} N c_{\text{SW}}$	89,560.64
ULA with HBF	$c_{\text{ULA}} = 3N_{\text{RF}} M c_{\text{PS}} + 3M c_{\text{An}}$	1,511,427.84
$c_{\text{cyl}}/c_{\text{ULA}} = 5.93\%$		

that the proposed cylinder DCAA can significantly reduce the hardware cost, amounting to only 5.93% of the required by the cell sectoring based on ULA with HBF. Sensitivity analysis indicates that the cylinder DCAA performs more cost-efficiently when the cost of an individual antenna element does not exceed \$ 54.2.

VII. CONCLUSION

In this paper, to solve the signal blockage problem inherent in RAA, we propose a novel architecture termed cylinder DCAA and its optimization algorithm for uplink and downlink communication. First, we analyze the characteristics of sUCA, which is the basic component of cylinder DCAA. Second, the cylinder DCAA's geometry structure is derived and the formulated expressions of its response pattern, uplink and downlink SINR and maximum sum rate are presented. Compared with ULA with HBF, cylinder DCAA has uniform spatial resolution, enhanced beamforming gain with directional antenna elements and substantial cost-efficiency. Based on the characteristics of cylinder DCAA, optimization algorithms to find the maximum sum rate in the uplink and downlink with greedy method or iteration-based method are proposed. Finally, the numerical results validate that cylinder DCAA has better sum rate performance than cell sectoring system based on ULA with HBF, especially in dense connectivity scenario, and the proposed algorithms are effective in finding the optimal power allocation with practical computational complexity together with good convergence performance. These inspirational findings demonstrate that the cylinder DCAA is a potential solution for the signal blockage problem of RAA. In the further work, we can explore lower complexity and more efficient algorithms for cylinder DCAA and some strategies of integrated sensing and communication (ISAC) for the communication system with cylinder DCAA.

APPENDIX A PROOF OF THEOREM 1

The amplitude of array factor $\text{AF}(\eta, \phi, \theta)$ in (14) is equivalently expressed as summarized weighted uniform complex

vectors given by:

$$|\text{AF}(\eta, \phi, \theta)| = \left| \sum_{m=1}^M \chi_m(\phi, \eta) \mathbf{u}_m(\eta, \phi, \theta) \right|, \quad (59)$$

where $\chi_m(\phi, \eta) = \sqrt{G(\xi_m(\eta), \psi)}$, $\mathbf{u}_m(\eta, \phi, \theta) = e^{jx_m(\eta, \phi, \theta)}$, ($m = 1, 2, \dots, M$) and $x_m(\eta, \phi, \theta)$ is given by:

$$\begin{aligned} x_m(\eta, \phi, \theta) &= \frac{4\pi}{\lambda} a \sin \theta \cos \left(\underbrace{\rho(\phi, \eta) - \frac{\pi}{M-1}(m-1)}_{\zeta(m, \phi, \eta)} \right) \sin(\rho(\phi, \eta)), \end{aligned} \quad (60)$$

where $\rho(\phi, \eta) = \frac{\phi - \eta}{2}$. Since $\rho(\phi, \eta) - \pi \leq \zeta(m, \phi, \eta) \leq \rho(\phi, \eta)$, the supremum and the infimum of the phase set relative to the index m is given by:

$$\begin{aligned} \sup_{1 \leq m \leq M} \{x_m\} &\approx \left| \frac{4\pi}{\lambda} a \sin \theta \sin(\rho(\phi, \eta)) \right| > 0 \\ \inf_{1 \leq m \leq M} \{x_m\} &= - \left| \frac{4\pi}{\lambda} a \sin \theta \cos(\rho(\phi, \eta)) \sin(\rho(\phi, \eta)) \right| < 0. \end{aligned} \quad (61)$$

From (61), the infimum of the set is negative and the supremum of the set is positive. Thus, there always exists a specific $1 \leq i_k \leq M$, such that $\zeta(i_k, \phi, \eta) \approx -\frac{\pi}{2}$. Based on the symmetric property of $\cos(\cdot)$ at the neighborhood of zero point, for a given angle set (ϕ, θ) , $\phi \in [\eta - \frac{\pi}{2}, \eta + \frac{\pi}{2}]$ and $\theta \in [0, \pi]$, there exists a sub-set of $2k$ vectors $\{\mathbf{u}_{i_1}, \mathbf{u}_{i_2}, \dots, \mathbf{u}_{i_{2k}}\} \subseteq \{\mathbf{u}_m\}$ that are symmetric relative to the real axis, i.e., $\angle \mathbf{u}_{i_j} + \angle \mathbf{u}_{i_{2k-j+1}} = 0, j = 1, 2, \dots, 2k$, where $M/2 \leq 2k \leq M$. Thus, complex uniform vector set is partitioned into two parts:

$$\begin{aligned} \{\mathbf{u}_m \mid m = 1, 2, \dots, M\} &= \underbrace{\{\mathbf{u}_{i_1}, \mathbf{u}_{i_2}, \dots, \mathbf{u}_{i_{2k}}\}}_{\text{symmetric part}} \underbrace{\{\mathbf{u}_{i_{2k+1}}, \mathbf{u}_{i_{2k+2}}, \dots, \mathbf{u}_{i_M}\}}_{\text{non-symmetric part}}. \end{aligned} \quad (62)$$

Thus, (59) is equivalently expressed to:

$$\begin{aligned} |\text{AF}(\eta, \phi, \theta)| &= \left| \underbrace{\sum_{j=1}^k (\chi_{i_j} \mathbf{u}_{i_j} + \chi_{i_{2k-j+1}} \mathbf{u}_{i_{2k-j+1}})}_{\triangleq \alpha} + \underbrace{\sum_{j=2k+1}^M \chi_{i_j} \mathbf{u}_{i_j}}_{\triangleq \beta} \right| \quad (63) \\ &= |\alpha - \beta^* + \beta + \beta^*| \stackrel{(a)}{\leq} |\alpha - \beta^*| + |\beta + \beta^*|, \end{aligned}$$

where (a) is based on Jensen's inequality. The maximum of (63) can only be obtained when $\angle(\alpha - \beta^*) = 0$. However, with the existence of non-symmetric vectors, i.e., $\phi \neq \eta$ and therefore $\beta^* \neq 0$, it is intuitive that $\angle(\alpha - \beta^*) \neq 0$. Thus, the maximum of (59) is obtained only at angle set $(\phi, \theta) = (\eta, \frac{\pi}{2})$. From (17), the beamwidth $\text{BW} = 2\phi_0 \approx 2\check{\phi}_0$. Thus, the proof of Theorem 1 is completed.

REFERENCES

- [1] X. Zhu, Z. Zhou, and Y. Zeng, "Full-Angle Ray Antenna Array and Omnicell Wireless Communication System," in *2025 IEEE Global Communications Conference, the 6th workshop on emerging topics in 6G communications*, accepted, 2025.
- [2] D. Tse and P. Viswanath, *Fundamentals of Wireless Communication*. Cambridge University Press, 2005.
- [3] C. Wang, X. You, X. Gao *et al.*, "On the Road to 6G: Visions, Requirements, Key Technologies, and Testbeds," *IEEE Commun. Surveys Tuts.*, vol. 25, no. 2, pp. 905–974, 2023.
- [4] Z. Xiao and Y. Zeng, "An overview on integrated localization and communication towards 6G," *Sci. China Inf. Sci.*, vol. 65, no. 3, p. 131301, 2022.
- [5] H. Lu, Y. Zeng, C. You *et al.*, "A Tutorial on Near-Field XL-MIMO Communications Toward 6G," *IEEE Commun. Surveys Tuts.*, vol. 26, no. 4, pp. 2213–2257, 2024.
- [6] X. Li, H. Min, Y. Zeng *et al.*, "Sparse MIMO for ISAC: New Opportunities and Challenges," *IEEE Wireless Commun.*, vol. 32, no. 4, pp. 170–178, 2025.
- [7] H. Q. Ngo, A. Ashikhmin, H. Yang *et al.*, "Cell-Free Massive MIMO Versus Small Cells," *IEEE Trans. Wireless Commun.*, vol. 16, no. 3, pp. 1834–1850, 2017.
- [8] Qorvo. TGP2102 32 - 37 GHz 5-Bit Phase Shifter. Accessed at: 2025-12-6. [Online]. Available: <https://www.qorvo.com/products/p/TGP2102>
- [9] Qorvo. TGS4302 High Power SPDT Switch. Accessed at: 2025-8-1. [Online]. Available: <https://www.qorvo.com/products/p/TGS4302>
- [10] Y. Zeng and R. Zhang, "Cost-Effective Millimeter-Wave Communications with Lens Antenna Array," *IEEE Wireless Commun.*, vol. 24, no. 4, pp. 81–87, 2017.
- [11] R. W. Heath, N. González-Prelcic, Rangan *et al.*, "An Overview of Signal Processing Techniques for Millimeter Wave MIMO Systems," *IEEE J. Sel. Top. Signal Process.*, vol. 10, no. 3, pp. 436–453, 2016.
- [12] Y. Zeng and R. Zhang, "Millimeter Wave MIMO With Lens Antenna Array: A New Path Division Multiplexing Paradigm," *IEEE Trans. Commun.*, vol. 64, no. 4, pp. 1557–1571, 2016.
- [13] L. Zhu, W. Ma, W. Mei, Y. Zeng *et al.*, "A Tutorial on Movable Antennas for Wireless Networks," *IEEE Commun. Surveys Tuts.*, pp. 1–1, 2025.
- [14] W. K. New, K.-K. Wong, H. Xu *et al.*, "A Tutorial on Fluid Antenna System for 6G Networks: Encompassing Communication Theory, Optimization Methods and Hardware Designs," *IEEE Commun. Surveys Tuts.*, vol. 27, no. 4, pp. 2325–2377, 2025.
- [15] M. R. Castellanos, S. Yang, C.-B. Chae, and R. W. Heath, "Embracing Reconfigurable Antennas in the Tri-hybrid MIMO Architecture for 6G and Beyond," *IEEE Trans. Commun.*, pp. 1–1, 2025.
- [16] W. Jiang, Q. Zhou, J. He *et al.*, "Terahertz Communications and Sensing for 6G and Beyond: A Comprehensive Review," *IEEE Commun. Surveys Tuts.*, vol. 26, no. 4, pp. 2326–2381, 2024.
- [17] L. Zhu, W. Ma, and R. Zhang, "Movable Antennas for Wireless Communication: Opportunities and Challenges," *IEEE Commun. Mag.*, vol. 62, no. 6, pp. 114–120, 2024.
- [18] Z. Dong, Z. Zhou and Y. Zeng, "Ray Antenna Array: A Novel Cost-Effective Multi-Antenna Architecture for Enhanced Wireless Communication," *accepted by 2025 VTC-spring*, 2025, available online: arXiv:2505.18163.
- [19] Z. Dong, Z. Zhou, and Y. Zeng, "A Novel Cost-Effective MIMO Architecture with Ray Antenna Array for Enhanced Wireless Communication Performance," *submitted to IEEE Trans. Wireless Commun.*, (major revision), 2025, available online: arXiv:2505.23394.
- [20] H. Jiang and Y. Zeng, "Ray Antenna Array Achieves Uniform Angular Resolution Cost-Effectively for Low-Altitude UAV Swarm ISAC," *submitted to IEEE Trans. Wireless Commun.*, (minor revision), 2025, available online: arXiv:2505.10306.
- [21] S. C. Dutta Roy, "Efficient Approximation of Variable Delay Using Tapped Delay Line," *Topics in Signal Processing: Analog and Digital*, pp. 49–53, 2020. [Online]. Available: https://doi.org/10.1007/978-981-13-9532-1_7
- [22] 3rd Generation Partnership Project (3GPP), *5G; Study on Channel Model for Frequencies from 0.5 to 100 GHz document 38.901, Version 19.1.0, Technical Report (TR)*. 3GPP, Sep. 2025.
- [23] S. Shi, M. Schubert, and H. Boche, "Downlink MMSE Transceiver Optimization for Multiuser MIMO Systems: Duality and Sum-MSE Minimization," *IEEE Trans. Signal Process.*, vol. 55, no. 11, pp. 5436–5446, 2007.
- [24] G. Scutari, D. P. Palomar, and S. Barbarossa, "The MIMO Iterative Waterfilling Algorithm," *IEEE Trans. Signal Process.*, vol. 57, no. 5, pp. 1917–1935, 2009.
- [25] Y. Han, S. Jin, J. Zhang, J. Zhang, and K.-K. Wong, "DFT-Based Hybrid Beamforming Multiuser Systems: Rate Analysis and Beam Selection," *IEEE J. Sel. Top. Signal Process.*, vol. 12, no. 3, pp. 514–528, 2018.
- [26] J. Fang, H. Liu, C. Xing *et al.*, "Hybrid Multiantenna Transceiver Optimizations for IoT Systems via Downlink–Uplink Duality," *IEEE Internet Things J.*, vol. 11, no. 5, pp. 8156–8169, 2024.